Forest Ecology and Management 497 (2021) 119497

Contents lists available at ScienceDirect

Forest Ecology and Management

journal homepage: www.elsevier.com/locate/foreco

Spaceborne height models reveal above ground biomass changes in tropical landscapes

Michael Schlund [a,*], Martyna M. Kotowska [b], Fabian Brambach [c], Jonas Hein [d], Birgit Wessel [e], Nicolò Camarretta [f], Mangarah Silalahi [g], I Nengah Surati Jaya [h], Stefan Erasmi [i], Christoph Leuschner [b,j], Holger Kreft [c,j]

[a] Department of Natural Resources, Faculty of Geo-information Science and Earth Observation (ITC), University of Twente, Hengelosestraat 99, Enschede 7514AE, the Netherlands
[b] Plant Ecology and Ecosystems Research, University of Göttingen, Untere Karspüle 2, Göttingen 37073, Germany
[c] Biodiversity, Macroecology & Biogeography, University of Göttingen, Büsgenweg 1, Göttingen 37077, Germany
[d] Department of Geography, Kiel University, Ludewig-Meyn-Str. 14, Kiel 24118, Germany
[e] German Remote Sensing Data Center (DFD), German Aerospace Center (DLR), Oberpfaffenhofen, Wessling 82234, Germany
[f] Bioclimatology, University of Göttingen, Büsgenweg 2, Göttingen 37077, Germany
[g] PT. REKI/Hutan Harapan, Jalan Dadali No.32, Bogor West Java and Bungku Village, Bajubang, atang Hari Regency, Jambi 36611, Indonesia
[h] Division of Forestry Planning, Department of Forest Management, Faculty of Forestry, Bogor Agricultural University, Jawa Barat 16680, Indonesia
[i] Thünen-Institute of Farm Economics, Bundesallee 63, Braunschweig 38116, Germany
[j] Centre of Biodiversity and Sustainable Land Use (CBL), University of Göttingen, Büsgenweg 1, Göttingen 37077, Germany

ARTICLE INFO

Keywords:
Aboveground biomass change
Height models
Interferometric synthetic aperture radar (InSAR) data
TanDEM-X
Tropical rainforest

ABSTRACT

The area-wide estimation of aboveground biomass (AGB) and its changes as a proxy for the sequestration and emission of carbon are currently associated with high uncertainties. Here we combined interferometric synthetic aperture radar (InSAR) height models derived from TanDEM-X with repeated ground-based inventories from the years 2012 and 2019 to estimate InSAR height and AGB changes in a structurally diverse and dynamic landscape in Sumatra, Indonesia. The results suggested that the InSAR height models were highly accurate and the relationship between InSAR height and AGB change resulted in a coefficient of determination R^2 of 0.65 and a cross-validated root mean square error (RMSE) of 2.38 Mg ha^{-1} year^{-1}, equivalent to 13.32% of the actual AGB difference range. The estimated AGB changes with TanDEM-X were further related to the initial canopy height and fire activities in the study area. Initial canopy heights and the occurrences of fires had a significant effect on the AGB change. In general, low canopy heights tend to be associated with increasing AGB over time, whereas high canopy heights tend to be associated with stable or decreasing AGB. As expected, fires had a negative impact on the AGB changes being more pronounced in forest areas compared to oil palm concessions. The results of this study are relevant for the utilization of spaceborne InSAR height models and its potential to estimate canopy height and AGB change on large spatial scales. It was demonstrated that these changes can be related to their sources and ecosystem processes. This AGB change estimation technique can be used to model the impacts of fires on AGB change and carbon emissions, which are important for sustainable forest management.

1. Introduction

Tropical landscapes are increasingly dominated by humans, even in formerly inaccessible tropical wilderness areas (Lewis et al., 2015; Venter et al., 2016; Watson et al., 2018). In the lowlands of South-East Asia, a highly dynamic mosaic of smallholder agriculture, large agribusiness plantations interspersed with patches of remnant forest and settlements have replaced the once extensive tropical rainforests (Lewis et al., 2015; Curtis et al., 2018; Austin et al., 2019). Management decisions are currently shaping the spatial and temporal dynamics of these landscapes with still unknown consequences for their ecological functioning and feedbacks on resource availability (Lawrence and Vandecar, 2015; Daskalova et al., 2020). Tropical landscapes are inherently considered for their role in fostering a staggering biodiversity and

* Corresponding author.
E-mail address: m.schlund@utwente.nl (M. Schlund).

https://doi.org/10.1016/j.foreco.2021.119497
Received 12 March 2021; Received in revised form 29 June 2021; Accepted 30 June 2021
Available online 13 July 2021
0378-1127/© 2021 The Author(s). Published by Elsevier B.V. This is an open access article under the CC BY license (http://creativecommons.org/licenses/by/4.0/).

supporting the livelihoods of local communities, but also for their contribution to global climate regulation through carbon sequestration and hydrological cycles (Chhatre and Agrawal, 2009; Malhi and Grace, 2000; Beer et al., 2010).

While deforestation, selective logging and forest degradation are major sources of greenhouse gas emissions from these tropical landscapes (van der Werf et al., 2009), the regrowth of secondary forest, agroforestry and tree plantations have the potential to mitigate some of the carbon losses through regrowth and carbon sequestration (Pan et al., 2011). However, the extent of this offset and the overall carbon balance of most human-modified tropical landscapes is unknown, as the dynamics of land use and carbon depend on a complex interplay of management decisions such as plantation conversion, selective logging, clear-cutting or slash-and-burn clearance with ecosystem processes such drought-induced mortality or pathogen outbreaks (Hudak et al., 2012). A better understanding of the influence of these drivers on AGB change is relevant for land use management and can be included in carbon modelling to predict future landscape dynamics and developments. This is particularly important in structurally diverse and dynamic landscapes (Brun et al., 2015).

Spatial estimates of AGB stocks and their changes over time are still associated with large uncertainties (Chen et al., 2015; Réjou-Méchain et al., 2019). One of the most promising option is to use remote sensing data to acquire information over large areas and calibrate and validate it with ground-based measurements (Réjou-Méchain et al., 2019). Consequently, the use of AGB estimates as proxies for carbon storage has been frequently studied in the past with different airborne as well as spaceborne sensors (Asner and Mascaro, 2014; Réjou-Méchain et al., 2015; Réjou-Méchain et al., 2019). However, obtaining precise AGB estimates for heterogeneous and dynamic landscapes is inherently difficult and most of the studies have to date focused on the estimation of the AGB at a single point in time in forest without considering other land use types (Cao et al., 2016).

The canopy height derived from active remote sensing techniques such as light detection and ranging (LiDAR) and synthetic aperture radar (SAR) are considered promising for the AGB estimation (Solberg et al., 2013; Asner and Mascaro, 2014; Réjou-Méchain et al., 2015; Schlund et al., 2020). It can be assumed that the information on canopy height is not only useful in estimating the AGB at a single point in time, but can also be used to detect and estimate AGB changes quantitatively. The AGB change can be estimated as the difference between two individual AGB estimations at different points in time, which represents an indirect AGB change estimation (McRoberts et al., 2015; Réjou-Méchain et al., 2015; Wedeux et al., 2020; Tompalski et al., 2021). Conversely, estimated differences in canopy height between different points in time are used to model AGB changes in the direct approach (McRoberts et al., 2015; Dubayah et al., 2010; Knapp et al., 2018; Karila et al., 2019; Tompalski et al., 2021).

Few studies have used airborne LiDAR sensors, which are generally able to estimate canopy surface as well as terrain height, to estimate the AGB change over time using either one or both approaches (Dubayah et al., 2010; Hudak et al., 2012; Meyer et al., 2013; Réjou-Méchain et al., 2015; Wedeux et al., 2020). However, airborne LiDAR sensors normally have a small spatial coverage and the data are relatively expensive for the end-user compared to spaceborne data, resulting in limited potential for consistent monitoring of AGB and its change. In addition, the settings of the flight and the LiDAR sensor often change between the airborne surveys, which potentially hinders a comparison and estimation of AGB change (Meyer et al., 2013; Wedeux et al., 2020). Spaceborne systems such as interferometric synthetic aperture radars (InSAR) are able to acquire data over large spatial extents with consistent settings to overcome the drawbacks of airborne LiDAR sensors. Spaceborne LiDAR systems such as GEDI and ICESat-2 can accurately estimate terrain heights, but are profiling instruments. In contrast, elevation models from InSAR data provide complete coverage to potentially detect unknown small-scale changes. However, to date there is no spaceborne InSAR system with the ability to estimate terrain height and thus canopy height in a spatially consistent and accurate manner. Consequently, the indirect approach is not possible with current spaceborne systems. The potential of InSAR X-band systems like SRTM and TanDEM-X to estimate the canopy surface height has long been recognized. The InSAR height has been frequently combined with terrain information from LiDAR to estimate the canopy height and subsequently AGB in different biomes (Solberg et al., 2013; Karila et al., 2019; Schlund et al., 2020). The canopy height is only available in the LiDAR coverage and thus is again spatially limited. Nevertheless, these studies show the potential of estimating the canopy surface height with TanDEM-X enabling the direct change approach. For instance, the interferometric heights can be used to detect forest disturbance (Lei et al., 2018). The direct method has been effectively applied in boreal areas to estimate AGB change quantitatively (Solberg et al., 2014; Karila et al., 2019), but its potential in the tropics has so far only been demonstrated conceptually (Solberg et al., 2015; Solberg et al., 2018). These studies assumed that the penetration of the X-band signal into the canopy is small and penetration depth differences are negligible, whereas a substantial penetration was observed in other studies depending on the acquisition parameters, forest structure and dielectric properties (e.g. moisture) (Kugler et al., 2014; Schlund et al., 2019). Penetration depth differences potentially propagate to pseudo-changes in a multi-temporal analysis and thus small changes due to growth or degradation might not be detectable (Karila et al., 2019). None of the former studies has to our knowledge deployed TanDEM-X InSAR height changes supplemented by ground-truth to detect large-scale biomass changes over time in the tropics linking them to potential drivers in a highly dynamic frontier of rainforest transformation.

In this study, we used repeated TanDEM-X digital elevation model (DEM) acquisitions and *in situ* inventory data from 2012 and 2019 to estimate the AGB change in this time frame across different land uses and forest management systems in a landscape of the Jambi province, Sumatra, Indonesia. The objectives of this study were to evaluate the potential of TanDEM-X InSAR height changes for estimating AGB changes in a tropical environment. A model to compensate for penetration depth and its differences over time was applied and its accuracy compared to InSAR heights without compensation (Schlund et al., 2019; Schlund et al., 2020). We further related the estimated landscape-level AGB changes to the initial vegetation height as a proxy of carbon stocks and investigated the role of detected fires as a relevant ecosystem process in different management systems (van der Werf et al., 2009; Ferraz et al., 2018).

2. Material and methods

2.1. Study area

The study was conducted in the tropical lowlands of Jambi Province on the Indonesian island of Sumatra, within the framework of the EF-ForTS (Ecological and Socioeconomic Functions of Tropical Lowland Rainforest Transformation Systems) project (Drescher et al., 2016). The climate is tropical humid with a drier period during July and August and with temperatures relatively constant throughout the year (26.7 °C, 2235 mm year^{-1}).

Large-scale conversion from the original rainforest vegetation to other land uses in Jambi Province started in the early 20th century with rubber (*Hevea brasiliensis*) agroforests and later rubber monocultures (Feintrenie and Levang, 2009). Deforestation has intensified since the early 1980s due to commercial logging, organized and spontaneous immigration, and the establishment of large-scale plantation agriculture of rubber, oil palm (*Elaeis guineensis*) and acacia (*Acacia mangium*). In the 2000s, a number of new national parks, protected areas and private conservation concessions were established, including the Harapan Rainforest as an ecosystem restoration area (PT REKI - PT Restorasi Ekosistem Indonesia) (Hein et al., 2016). Today, the study area consists

of a highly dynamic mosaic landscape of natural remnant rainforest patches, various smallholder plantations and company-owned plantation estates and concessions (Laumonier et al., 2010; Clough et al., 2016) (Fig. 1). For the purpose of this study, the study area was separated into three land categories with distinct management, namely (1) protected area (Hutan Harapan), (2) large-scale oil palm concessions and (3) remaining land, mainly managed as smallholder plantations.

2.2. Material

2.2.1. Remote sensing data

In this study, TanDEM-X data were used, which was acquired using two SAR satellites with each sensor utilizing a phased-array X-band (i.e. 3.1 cm wavelength) antenna to transmit and receive the electromagnetic waves. The close formation of the TanDEM-X mission enables the acquisition of single-pass InSAR data to create global DEMs (Krieger et al., 2007). Two single-pass InSAR datasets with a time difference of about 6.3 years, October 30, 2012 and February 25, 2019, were used in this study, which were spatially and temporally consistent with forest plot inventory data. The TanDEM-X data were acquired in horizontal polarization (transmit and receive, HH) and in bistatic StripMap mode resulting in a resolution of about 3 m (Table 1). The spectrally filtered and co-registered CoSSC (co-registered single-look slant range complex) data products were used in this study (Fritz, 2012).

Table 1
Summary of TanDEM-X datasets (incidence angle θ, height of ambiguity (HoA) and effective baseline are for scene center).

Acquisition date	θ (°)	Resolution (m) azimuth × range	HoA (m)	Effective baseline (m)	Orbit
October 30, 2012	34.7	3.3 × 3.1	38.4	141.7	Descending
February 25, 2019	32.3	3.3 × 3.3	46.6	107.5	Ascending

The two acquisitions were part of the global TanDEM-X DEM and change DEM acquisition phase (Lachaise et al., 2019). The height of ambiguities were comparable with 38.4 m and 46.6 m and thus resulted in similar height sensitivity and performance.

Airborne LiDAR data were available for two sites in the study area (Fig. 1). The data were acquired in January, 2020 with a Riegl Q780 full waveform scanner with a nominal pulse density of 15 points/m^2. According to the provider, the data had a fundamental vertical accuracy of $\leq$ 10cm. The LiDAR data covered an area of 192 km^2, which was about 20% of the total study area of 985 km^2.

Digital surface (DSM) and digital terrain models (DTM) were derived

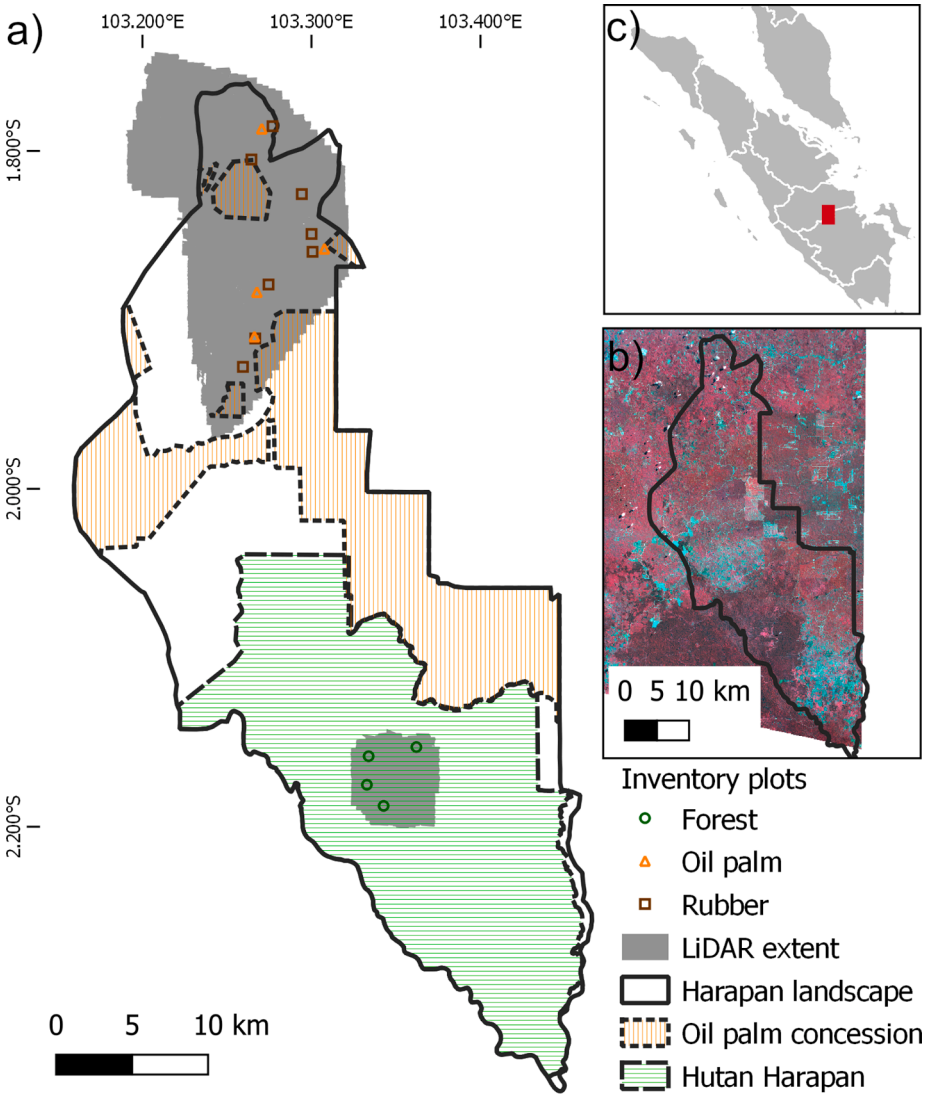

Fig. 1. Overview of the study area with the location of field inventory plots, the LiDAR extent and land categories (a) as well as a Landsat-8 false-color image from August 15, 2019 (b) on the island of Sumatra, Indonesia (c) (R = Near-infrared, G = Red, B = Green; Landsat-8 image courtesy of the U.S. Geological Survey).

from the 3D-point cloud of the LiDAR data. First, the point cloud was denoised where isolated points of the point cloud were removed. The denoised point-cloud was further classified to ground and non-ground points. Finally, the ground points and maximum height of all points within a grid cell of 1 m were triangulated to rasters of DTM as well as DSM. The rasters were resampled to the TanDEM-X InSAR height pixel size of 6 m in order to enable the comparison of these different datasets.

In addition to the remote sensing data to derive height information (i.e. InSAR and LiDAR data), the active fire product from the Visible Infrared Imaging Radiometer Suite (VIIRS) on board the Suomi National Polarorbiting Partnership (S-NPP) satellite was used in this study (Schroeder et al., 2014). This product has a spatial resolution of 375 m detecting fires with a multi-spectral contextual algorithm. This algorithms aims to identify sub-pixel fire activity and other thermal anomalies and was developed based on the experience with the MODIS Fire and Thermal Anomalies product (Giglio et al., 2003; Schroeder et al., 2014). Only fires detected between October 30, 2012 and February 25, 2019 were used in this study to assess the role of fires in the monitoring period as relevant ecosystem process and potential indicator for carbon stock changes. About 66% of the fires occurred in the second half of 2015, which coincides with the El Niño-Southern Oscillations (ENSO) event from 2015 and 2016.

2.2.2. Field inventory of aboveground biomass and its changes

To compare *in situ* AGB inventory data with spaceborne estimates from TanDEM-X height models, the AGB change was assessed on 16 plots with a size of 50 m × 50 m (0.25 ha). The plots were located with a multi-band/multi-system GNSS (global navigation satellite system) receiver with an estimated accuracy generally below 5 m within the three prevalent land use types occurring in this area, namely rubber plantations, oil palm monocultures and natural rainforest subjected to selective logging in the past. The inventory plots were homogeneous in overall environmental conditions like topography (flat) and soil (loam Acrisols), but captured the variability of land cover representative for the study area (Drescher et al., 2016). The plot locations with the tree information were visually compared to the remote sensing data to confirm the spatial consistency between the datasets. Plant species identity and structural variables - tree height and diameter at breast height (dbh) - of all trees with a dbh ⩾10 cm were repeatedly measured in 2012 and 2019 following the protocol described in Kotowska et al. (2015). Tree height was recorded using a Vertex III height meter (Haglöf, Långsele, Sweden) and measuring tapes (Richter Measuring Tools, Speichersdorf, Germany) were used for the diameter. Oil palm height was defined as the length from the base of the trunk to the base of the youngest leaf. The management of the plantation included application of herbicides, occasional weeding and irregular addition of inorganic NPK fertilizer. The AGB of each tree in rainforest and rubber plots was estimated using the allometric equation by Chave et al. (2014) within the BIOMASS-package (Réjou-Méchain et al., 2017) where wood density was estimated from tree species identity using the global wood density database as a reference (Chave et al., 2009; Zanne et al., 2009), and for oil palms following the allometric equation given by Khasanah et al. (2015). The individual tree AGB estimates were summed and areal normalized to Mg ha^{-1} (Table 2). Annual AGB changes per hectare were calculated as the difference in summed AGB data of each site between the census dates including recruitment and mortality of trees that occurred in-between.

Table 2
Summary of field inventory data with the average diameter at breast height (DBH), tree height and AGB (standard deviation in brackets).

Date of inventory	Number of repeated plots	Plot size (ha)	DBH (cm)	Tree height (m)	AGB (Mg ha^{-1})
2012	16	0.25	32.6 (24.6)	13.1 (5.6)	149.49 (121.36)
2019	16	0.25	32.5 (21.6)	16.4 (5.7)	176.57 (115.09)

2.3. Methods

2.3.1. InSAR height retrieval

The individual InSAR heights were retrieved on the basis of complex interferograms. The complex interferograms of each individual TanDEM-X CoSSC data pair were calculated, where a multi-looking was applied to result in 6 m pixel spacing. The phase of the flat earth was removed and interferometric coherence γ was estimated from the individual CoSSC data pairs with an estimation window of 11 by 11 pixels (Rizzoli et al., 2017). The wrapped phase was unwrapped with the minimum cost flow algorithm and further refined to absolute topographic phase (Fritz et al., 2011; Rossi et al., 2012; Lachaise et al., 2019). The absolute topographic phase was converted to topographic (ellipsoidal) InSAR heights h_{InSAR}, which were finally geocoded and resampled to 6 m spacing. Each individual CoSSC data pair was processed in a similar way using the Integrated TanDEM-X Processor (ITP) and Mosaicking and Calibration Processor (MCP) from the German Aerospace Center (DLR) (Gruber et al., 2012; Rossi et al., 2012). This procedure guaranteed an accurate absolute height calibration of the InSAR heights (Wessel et al., 2018). However, the absolute accuracy of the InSAR height model from February 28, 2019 was also empirically assessed in non-vegetation areas with the respective LiDAR height model, where non-vegetated areas were defined with a canopy height below 1 m.

The penetration depth of the individual TanDEM-X acquisitions in vegetation potentially differed due to different acquisition properties. This could result in a pseudo-change in the comparison of the individual InSAR heights (Schlund et al., 2019; Schlund et al., 2020). Consequently, the penetration depth h_{Depth} was estimated based on the respective volume coherence and height of ambiguity of each individual acquisition. The volume coherence was derived from the interferometric coherence γ

$$\gamma_{\mathrm{Vol}} = \frac{\gamma}{\gamma_{\mathrm{SNR}}} \tag{1}$$

assuming that the signal-to-noise ratio coherence γ_{SNR} and the volume coherence γ_{Vol} were the main contributions to the interferometric coherence (Kugler et al., 2014; Schlund et al., 2019). The signal-to-noise ratio was calculated for each pixel based on their backscattering coefficient and the noise equivalent sigma zero (NESZ), which describes the noise from the antenna pattern and the antenna's thermal noise (Kugler et al., 2014; Schlund et al., 2019). The penetration depth estimation was based on an assumed link of the phase of the normalized interferometric coherence and the penetration depth, where the coherence phase has a unique relationship to the coherence magnitude in infinite volumes (Dall, 2007). This relationship was finally used to estimate the penetration depth of the individual TanDEM-X acquisitions (Schlund et al., 2019). The estimated penetration depth was calculated pixelwise with respect to the individual InSAR heights resulting in a penetration depth compensated InSAR height for each acquisition. The absolute accuracy of the InSAR height from February 28, 2019 was also assessed in vegetated areas. The original InSAR height as well as the penetration depth compensated InSAR height was compared to the LiDAR surface height, where vegetated areas were defined with a canopy height above 5 m.

The InSAR height changes were estimated via calculating the difference of the individual InSAR height compensated for its penetration depth $\Delta h_{\mathrm{InSARc}}$

$$\Delta h_{\mathrm{InSARc}} = (h_{\mathrm{InSARt2}} - h_{\mathrm{Depht2}}) - (h_{\mathrm{InSARt1}} - h_{\mathrm{Depht1}}) \tag{2}$$

where h_{InSARti} means the topographic height retrieved from TanDEM-X InSAR data with respect to the ellipsoid at time step 1 and 2 and h_{Depthti} means the estimated penetration depth defined as negative value.

The InSAR height differences were also calculated without their penetration depth estimation to assess the effect of the difference in penetration Δh_{InSAR}

$$\Delta h_{InSAR} = h_{InSARt2} - h_{InSARt1} \quad (3)$$

2.3.2. Spaceborne AGB change estimation

Previous studies have revealed a linear relationship of canopy height models h_{CHM} and AGB (Solberg et al., 2013; Schlund et al., 2020), where the InSAR height h_{InSAR} can be used together with a terrain model $h_{Terrain}$ to estimate a canopy height model, especially after compensating for the penetration depth (Schlund et al., 2019; Schlund et al., 2020)

$$AGB = a + b \cdot h_{CHM} = a + b \cdot (h_{InSAR} - h_{Terrain}) \quad (4)$$

where a and b correspond to the model coefficients of this linear model. This allows to calculate the AGB change ΔAGB as the difference of the individual AGB estimations (i.e. indirect approach). However, a terrain model is not available for the majority of the study area (and in general in majority of the Earth) and thus this approach was not used in this study. Instead, the annual InSAR height difference Δh_{InSAR} was related with the annual AGB difference ΔAGB as a linear model (i.e. direct approach). Differentiating the linear model of canopy height h_{CHM} and AGB from Eq. (4) results in a change estimation without intercept

$$\frac{dAGB}{dh_{CHM}} = b \quad (5)$$

$$\Delta AGB = b \cdot \Delta h_{CHM} = b \cdot ((h_{InSARt2} - h_{Terrain}) - (h_{InSARt1} - h_{Terrain})) = b \cdot \Delta h_{InSAR} \quad (6)$$

This model was independent of the terrain height information (i.e. the terrain information is cancelled out in the difference calculation). The model from Eq. (6) was fitted using the mean values of the penetration compensated Δh_{InSARc}, and non-compensated InSAR height Δh_{InSAR} separately within the inventoried plots and their AGB change information. The annual differences were retrieved by dividing the AGB and InSAR height difference with their temporal separation in years (i.e. 6.3 years). Note that this model had no intercept, where additionally a model with intercept was also established to test the potential effect of an intercept.

The coefficient of determination R^2 was calculated where an adjustment factor was introduced to account for the regression model without intercept (Kvalseth, 1985). The significance of the linear regressions were estimated using the F-test and the corresponding p-values. The number of repeated inventoried plots was too small to create an explicit validation data set. Therefore, a k-fold cross-validation was used to assess the goodness of the models, where k was set to the number of observations resulting in a leave-one-out cross-validation. The root mean square error (RMSE) was calculated and averaged for all subsamples in the cross-validation. Further, the mean error (ME) was calculated to indicate a potential bias resulting in an under- or over-estimation of the AGB change estimation, where negative values would indicate an under- and positive values an over-estimation of the prediction.

2.3.3. Analysis of effects on aboveground biomass dynamics

The InSAR height difference was aggregated to 0.25 ha pixels similar to the inventory plot size and the AGB change was estimated spatially using the linear model of Eq. (6). It can be assumed that the initial height as well as fire occurrences have a substantial influence on AGB dynamics in natural forests (Knapp et al., 2018; Wedeux et al., 2020). The canopy height based on the difference between the penetration compensated TanDEM-X InSAR height models and the digital terrain model from LiDAR was calculated for both dates assuming that the terrain height was constant for 2012 and 2019. The InSAR height model of the first date was used to assess the effect of the initial canopy height on AGB dynamics. This information was also resampled to 0.25 ha to enable a pixelwise comparison with the spatial AGB change information. The distance from detected fires based on VIIRS was also calculated for each 0.25 ha pixel. Splines were fitted between the AGB change and the two variables, initial canopy height and distance from fires, for a visual interpretation of the relationships.

It can be assumed that fires had a different impact on AGB dynamics in different land use systems. Therefore, the effect of fires were assessed in the three land categories, (1) protected area (Hutan Harapan), (2) large-scale oil palm concessions and (3) remaining land (see Section 2.1). A two-sample t-test was used to assess the difference of AGB change in these three land categories. The effect of initial canopy height could only be studied in the LiDAR coverage, which covered mainly the smallholder landscape and parts of the rainforest area (Fig. 1). Furthermore, linear mixed-effects models were fitted in the LiDAR coverage to assess AGB gains and losses with respect to their initial canopy height and distance from fires. These models included the initial canopy height CHM_{2012} and distance from fires D_{Fires} individually and their combination as a (multiple) linear mixed-effects model. In addition, the variables were also scaled to a mean of 0 and a standard deviation of 1 prior the fit of the linear mixed-effects model. Therefore, the coefficients represent the relative strength of the different variables in the model with the scaled variables. An exponential correlation structure based on the geo-coordinates of each data point was used in the linear mixed-effects models to account for spatial autocorrelation (Mets et al., 2017; Wedeux et al., 2020). The coefficient of determination R^2 was calculated for all the mixed-effects models according to Nakagawa et al. (2017) to indicate the explained variance of the relationship. Furthermore, the proportion of explained variance of initial canopy height and fires on AGB change was estimated by calculating the ratio of the sum of squares of the individual effects with the cumulative sum of squares of the individual effects in an analysis of variance (ANOVA). This analysis was implemented in the R environment with the support of the *nlme* and *performance* package (R Core Team, 2021; Pinheiro et al., 2021; Lüdecke et al., 2021).

3. Results

3.1. Accuracy of TanDEM-X InSAR height models

The TanDEM-X InSAR height achieved an RMSE of 3.46 m in comparison with the LiDAR height in non-vegetated areas. The ME was about −0.53 m, which suggested a small underestimation in non-vegetated areas. The two different heights resulted in a significant linear relationship with a coefficient of determination of 0.96 and a p-value below 0.001 (Fig. 2).

The comparison in vegetated areas revealed also a significant (p-value< 0.001) linear relationship between the InSAR height and LiDAR height, where the R^2 was 0.93 for both InSAR heights, original and penetration depth compensated. A systematic bias was observed in the original InSAR height resulting in an ME of −6.7 m and an RMSE of 7.8 m. The accuracy improved to an ME of −1.1 m and an RMSE of 4.3 m after the compensation for the penetration depth (Fig. 2).

3.2. Aboveground biomass change in the study area

The AGB of the repeated inventoried plots ranged from 46.53 Mg ha^{-1} to 393.32 Mg ha^{-1} in 2012 across all land use systems. The AGB increased during the monitoring period in most of the plots. The gain in the inventoried plots ranged between 2.04 Mg $ha^{-1}year^{-1}$ to 11.07 Mg $ha^{-1}year^{-1}$, where two rubber plots had a loss of −3.80 Mg $ha^{-1}year^{-1}$ and −1.30 Mg $ha^{-1}year^{-1}$ respectively. One forest plot was also subject to a substantial AGB loss of about −6.79 Mg $ha^{-1}year^{-1}$ (Fig. 3).

The gain and loss of AGB was also reflected in the gain and loss of TanDEM-X InSAR height between 2012 and 2019. The oil palm

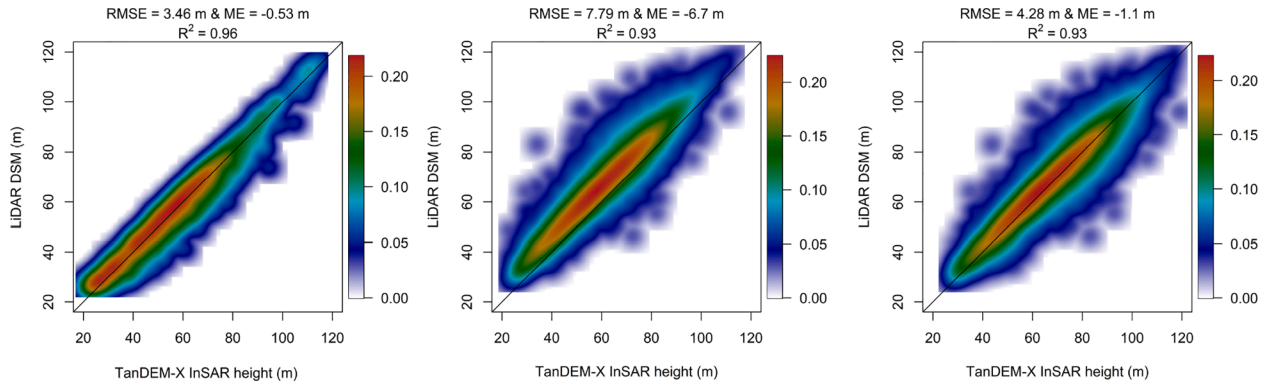

Fig. 2. Colored density representation of scatterplots with TanDEM-X InSAR heights in not-vegetated areas (left), InSAR height in vegetated areas (center) and InSAR height with penetration depth compensation in vegetated areas (right) in comparison to LiDAR DSM.

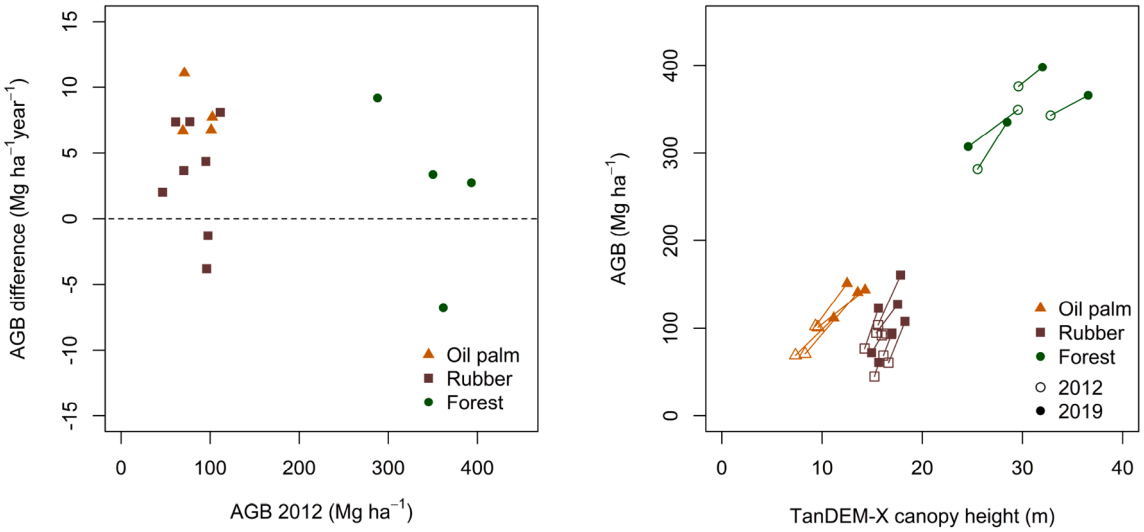

Fig. 3. Aboveground biomass difference between 2012 and 2019 in relation to the initial aboveground biomass in 2012 (left) and comparison of aboveground biomass and TanDEM-X based canopy height models with penetration depth compensation in 2012 and 2019 (right).

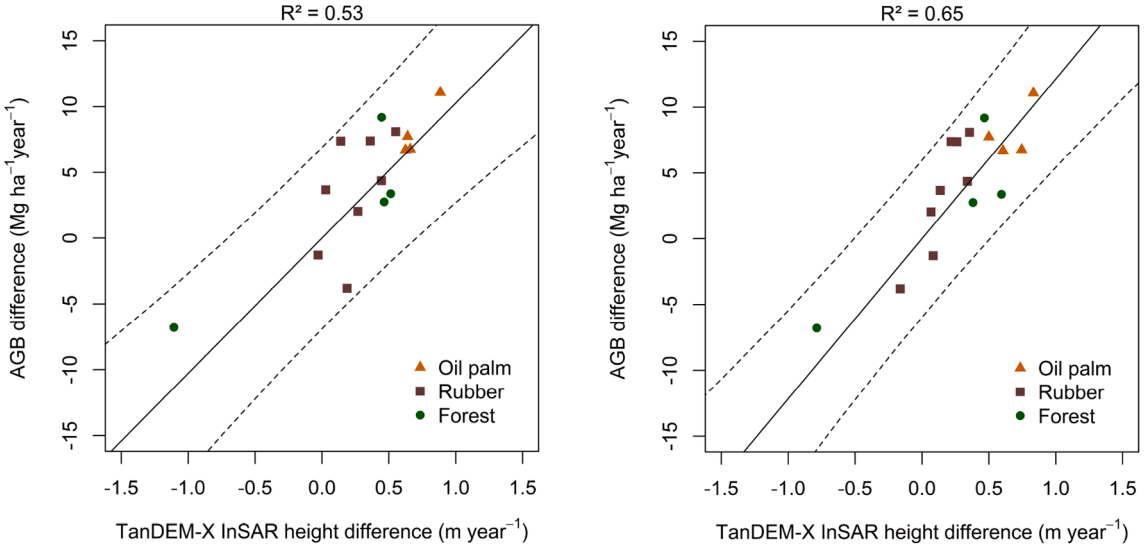

Fig. 4. Linear relationship between AGB differences and original TanDEM-X InSAR height differences (left) and penetration depth compensated TanDEM-X InSAR height differences (right).

plantations resulted in the largest gain of AGB, while the analysis revealed also a gain of 2.73 m to 4.30 m InSAR height in these plots. The rubber and rainforest plots indicated generally a small gain when comparing the InSAR based canopy height values of 2012 and 2019, whereas one forest plot showed a substantial loss of 8.29 m InSAR height (Fig. 3).

The yearly differences of TanDEM-X height with and without penetration compensation and AGB revealed a significant linear relationship ($p < 0.001$) (Fig. 4). The coefficients of determination were 0.53 for the InSAR without penetration depth compensation and 0.65 with the compensation for penetration depths. The penetration compensated InSAR heights resulted not only in a higher R^2, but also in a smaller prediction interval (Fig. 4). The slope coefficients of these linear relationships without intercept were 10.27 ($p < 0.001$) without compensation and 12.15 ($p < 0.001$) with compensation. Note that the additional model with intercept resulted in a insignificant intercept ($p > 0.1$) and similar R^2 and slope values. The estimation of AGB change with the original InSAR heights (without compensation) resulted in a cross-validated ME of -1.03 Mg ha^{-1}year^{-1} and an RMSE of 2.69 Mg ha^{-1}year^{-1}, whereas the compensated InSAR heights resulted in an ME of -0.77 Mg ha^{-1}year^{-1} and an RMSE of 2.38 Mg ha^{-1}year^{-1}. These RMSE values were equivalent to 15.09% and 13.32% of the actual AGB difference range. Largest discrepancies were observed in the extremes of the gains, whereas the *in situ* plots with losses and small gains were generally aligned on the regression line.

The AGB differences up-scaled to the study area were generally normally distributed with a mean of -2.70 Mg ha^{-1}year^{-1} and a standard deviation of 11.88 Mg ha^{-1}year^{-1}. However, a kurtosis around -25 Mg ha^{-1}year^{-1} was observed (Fig. 5). The separation in the different land categories (i.e. rainforest, oil palm concession and smallholder plantations) revealed that this kurtosis was based on a substantial AGB loss in oil palm concessions (Fig. 5). In general, the t-test revealed that the land categories were significantly different in their AGB change. The protected forest areas generally had more negative AGB changes than the other two land categories and it had on average a loss of -5.79 Mg ha^{-1}year^{-1} with a standard deviation of 13.91 Mg ha^{-1}year^{-1}. In contrast, the peak of the density in the other two land categories was around 0 Mg ha^{-1}year^{-1}, which resulted in a mean of -2.53 Mg ha^{-1}year^{-1} for oil palm concessions and -0.70 Mg ha^{-1}year^{-1} for smallholder plantations. The standard deviation for both land categories (i.e. oil palm concession and smallholder plantations) was 11 Mg ha^{-1}year^{-1}.

3.3. Effect of initial canopy height and fires on aboveground biomass difference

The average AGB loss of -2.17 Mg ha^{-1}year^{-1} and the kurtosis of the density plot at -25 Mg ha^{-1}year^{-1} in oil palm concessions was mainly based on a large oil palm concession area in the center of the study area, where after the end of the production cycle, the palms were cleared for re-planting (Fig. 6). Overall, the AGB did not change substantially in the oil palm concession areas with a low number of detected fires in these areas. In contrast, a large number of fires were detected in the north-west of the Hutan Harapan and in north-west of the study area. This area belongs to the third land category besides protected area and oil palm concessions and consists mainly of smallholder plantations. The highest negative differences were spatially consistent with the detected active fires from VIIRS (Fig. 6). The smallholder land category included also areas with stable AGB and even substantial AGB increase in the west of the study area. In contrast, negative AGB changes were generally visible in the Hutan Harapan area, which were highest at the northern border of the protected area consistent with the detected fires (Fig. 6).

The dependence of the annual AGB change on the proximity to fires was confirmed in the visualization of the trends between AGB change and distance from fires. As expected, pixels closest to fires tended to have negative AGB change, whereas the trend of the fitted spline was positive with increasing distance from fires (Fig. 7). In addition, the initial canopy height was also relevant for the AGB change, where on the one hand pixels with lower initial canopy heights tended to have a positive AGB change. On the other hand, the AGB tended to decrease in pixels with higher canopy heights (Fig. 7).

The trend identified from the visual interpretation was confirmed in the individual models of the relationship between AGB change ΔAGB and initial canopy height CHM_{2012} and distance from fires D_{Fires} showing the influence of initial canopy height and distance to fires on AGB change. The coefficient of determination was 0.14 and the slope coefficient was -0.45 for the model with AGB change and initial canopy height (Table 3). The slope coefficient was positive in the relationship of AGB change and distance from fires. However, the coefficient of determination for this model indicated a weaker relationship compared to the model with the canopy height from 2012. The stronger effect of the initial canopy height was confirmed in the multiple linear mixed-effects model with scaled variables, where the coefficient of the distance from fires was closer to zero than the coefficient of the canopy height (Table 3). The R^2 of this model was 0.16, where the proportion of explained variance indicated by the sum of squares of the individual effects in the ANOVA revealed that the initial height explained about 90.9% and fires 9.1% of the explained variance. All models and

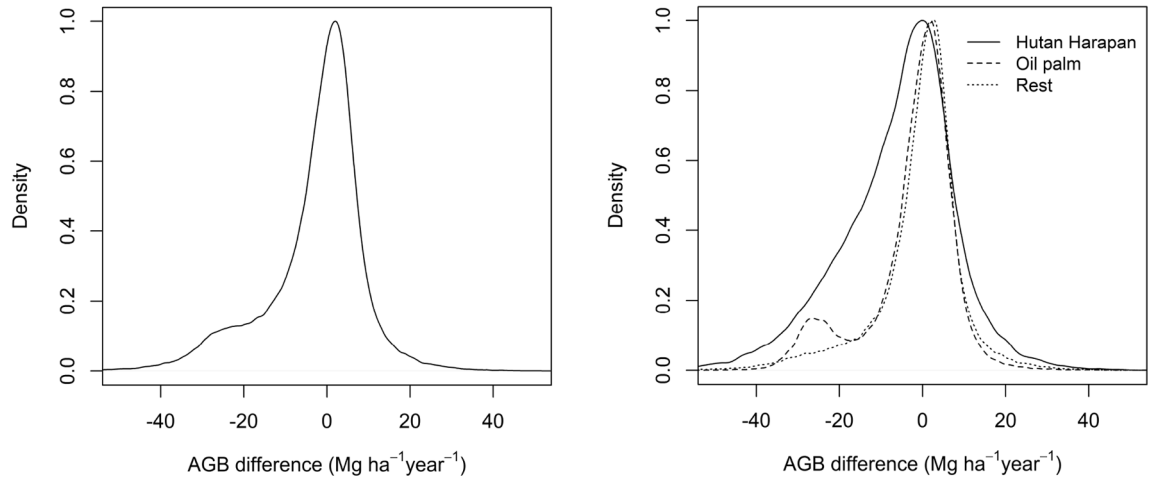

Fig. 5. Density plots of estimated aboveground biomass difference estimated with penetration depth compensated TanDEM-X InSAR height differences in study area (left) and in different land categories of the study area (right).

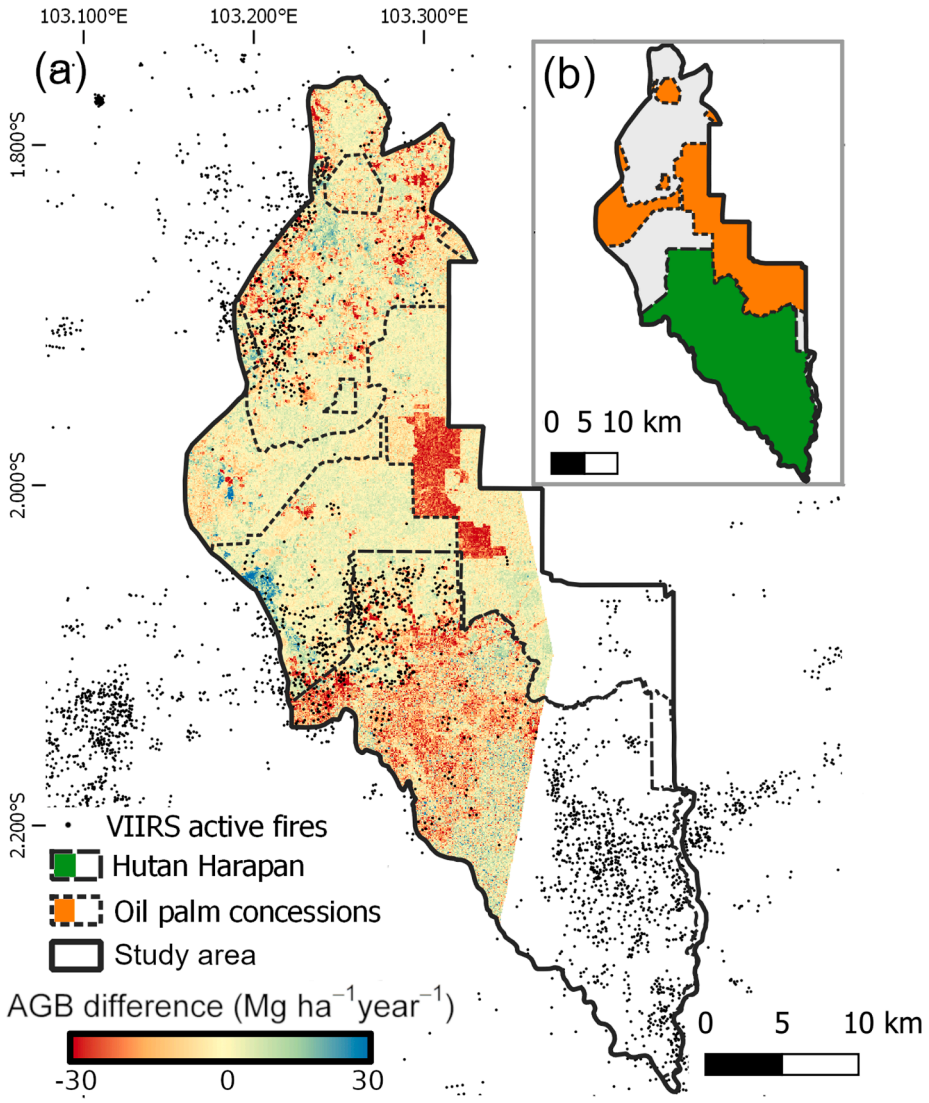

Fig. 6. Spatial representation of annual aboveground biomass change estimated with penetration compensated TanDEM-X InSAR height models with VIIRS active fire detections between October 30, 2012 and February 25, 2019 (a) and overview of land categories in the study area to support the visual interpretation (b).

coefficients were considered significant with a p-value < 0.001.

The spatial representation of AGB change and active fires indicated differences in the spatial distribution of fires and AGB changes. This was also visible in the visualization of the trends between AGB change and distance from fires in the individual land categories. In general, the majority of the pixels had a distance from 0 m to 500 m from fires in the Hutan Harapan area, where most of them indicated a negative change (Fig. 8). Consequently, there was a trend with negative changes close to fires to no change with increasing distance from fires. A similar but less obvious trend indicated by the fitted spline was observed in the other land category including mainly smallholder plantations. The majority of pixels had a distance from fires of 0 m to 1500 m in this land category. The trend indicated by the spline was horizontal, indicating independence of AGB changes on the distance from fires after a distance of about 500 m (Fig. 8). The distance from fires in the oil palm concessions was generally higher compared to the rainforest and the other land category. The majority of the pixels had a distance of 500 m to 3500 m. Consequently, the fitted spline indicated no trend between AGB change and distance from fires (Fig. 8).

4. Discussion

4.1. Estimation of aboveground biomass change with TanDEM-X

Our study illustrates the high potential of TanDEM-X height models and their change to estimate AGB change, which was confirmed by a significant relationship between the TanDEM-X InSAR height and AGB changes with an R^2 of 0.65. This relationship resulted in a cross-validated RMSE of 2.38 Mg ha^{-1} year^{-1}, which was equivalent to 13.32% of the actual AGB difference range. It is worth noting that the approach used here does not depend on a classification of changes in e.g. deforestation and forest degradation, since it estimates the stocks directly (Solberg et al., 2015). The quantitative demonstration in tropical areas was to date limited to a TanDEM-X coherence based height inversion with the support of LiDAR data in a mature forest with small changes resulting in high uncertainties (Knapp et al., 2018). Note that the height in Knapp et al. (2018) was based on the inversion of interferometric coherence to canopy height and thus it is a substantially different approach to the interferometric height differences used in our study. In addition, sufficient variation in the observed changes of canopy height and AGB were considered highly relevant for an accurate

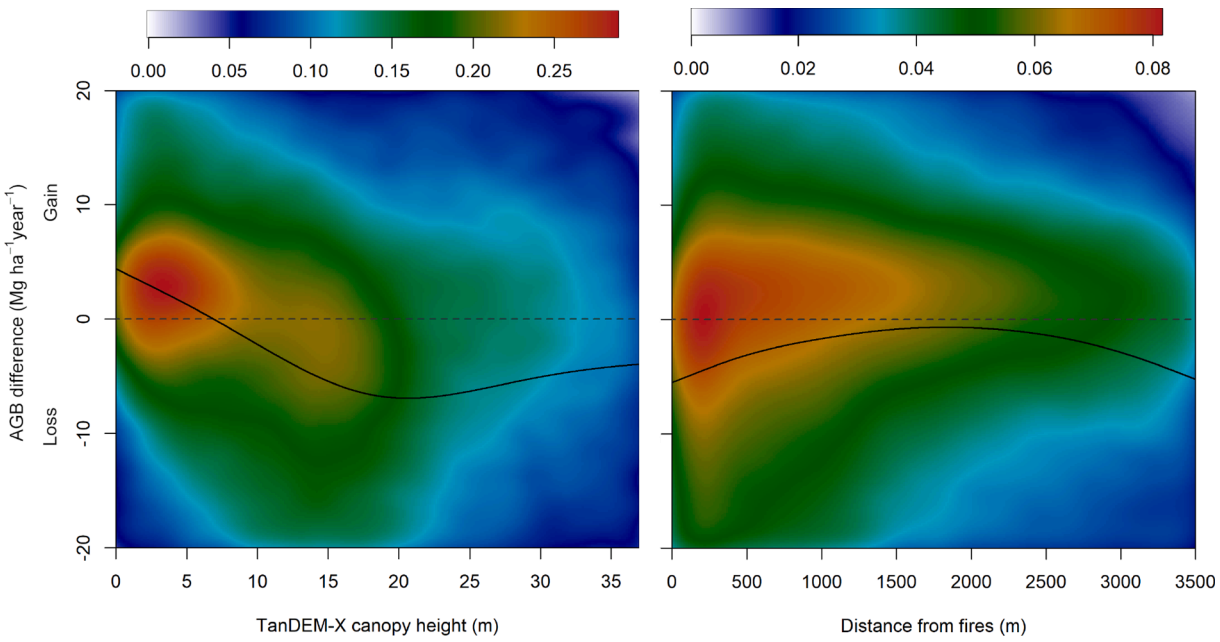

Fig. 7. Colored density plots of annual aboveground biomass change estimated with penetration compensated TanDEM-X InSAR height models and the initial TanDEM-X canopy height (left) as well as the distance from active fires (right) with fitted splines.

Table 3
Estimates of coefficients of determination and coefficients in linear mixed-effects models of AGB change in relation to canopy height and distance from fires including a geo-coordinate based exponential correlation structure to account for spatial autocorrelation (all terms were significant with $p < 0.001$).

Model	R^2	a	b	c
$\Delta AGB = a + b \cdot CHM_{2012}$	0.14	3.30	−0.45	
$\Delta AGB = a + b \cdot D_{Fires}$	0.03	−4.02	0.002	
$\Delta AGB = a + b \cdot CHM_{2012} + c \cdot D_{Fires}$	0.16	0.65	−0.46	0.003
$\Delta AGB = a + b \cdot CHM_{2012Scale} + c \cdot D_{FiresScale}$	0.16	−1.80	−3.71	1.72

estimation of AGB change (Dubayah et al., 2010). Our study had a large variation in terms of initial canopy height and AGB as well as their change covering also different forest and land use systems, where the high potential of TanDEM-X InSAR height changes for the estimation of AGB changes was confirmed. The estimation of absolute AGB with TanDEM-X based canopy heights and linear models suggested also a linear model for the change estimation as demonstrated in Eq. (6) (Solberg et al., 2013; Karila et al., 2019; Schlund et al., 2020). This was not in contrast to individual tree based allometries, where a power-law relationship is normally used to estimate AGB, because the InSAR heights were an areal metric aggregated to the plot level (Asner and Mascaro, 2014). Consequently, the InSAR heights were determined by the canopy density and height, which can be assumed linearly proportional to the AGB (Treuhaft and Siqueira, 2004; Solberg et al., 2013).

It is worth noting that the model without intercept was confirmed empirically by the fact that an intercept in Eq. (6) was insignificant ($p > 0.1$). A model without intercept implies the adequate assumption that zero height change results in zero AGB change. This was also suggested in other studies where the intercept was considered insignificant (Knapp et al., 2018; Karila et al., 2019). The slope as well as the accuracy of the linear model to estimate AGB change differed between penetration depth compensated and not-compensated InSAR height models. This confirmed the relevance of penetration depth compensation to make the individual InSAR heights comparable. The slope of the linear models varied also compared to other studies conducted in a boreal

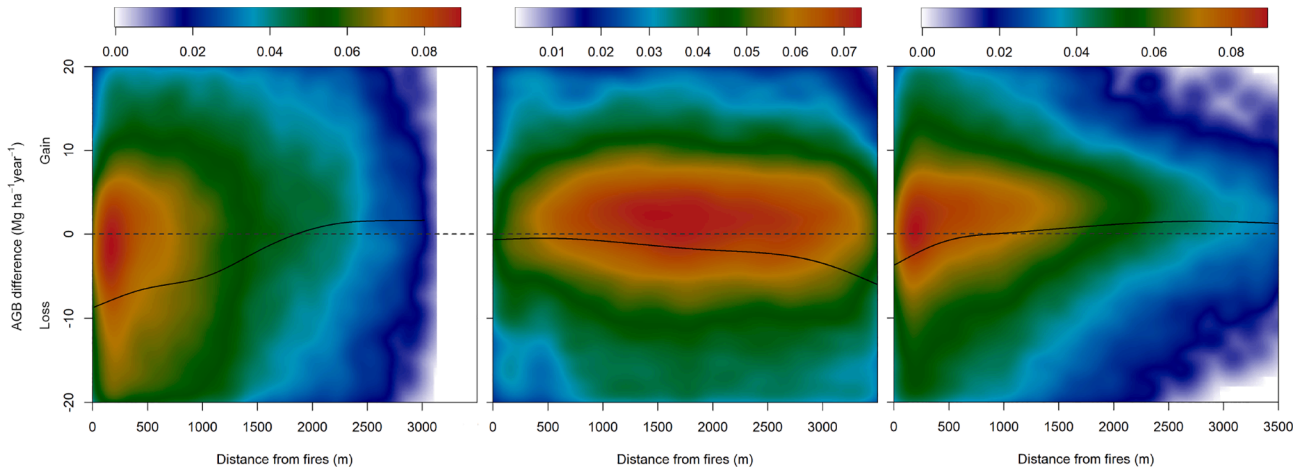

Fig. 8. Colored density plots of annual aboveground biomass change estimated with penetration compensated TanDEM-X InSAR height models and the distance from active fires with fitted splines in Hutan Harapan (left), oil palm concessions (center) and other land categories (right).

forest, where a slope of 6.39 and 6.90 were reported depending on the reference area (Karila et al., 2019). Steeper slopes were found in the tropical area of our study, in simulations of tropical forests depending on the time interval and in another boreal area (Knapp et al., 2018; Solberg et al., 2014). This suggests that the linear model of InSAR height change and AGB change is generally site dependent, which was also found in the estimation of absolute AGB (Schlund et al., 2020). However, the penetration depth compensation enabled the comparison to LiDAR data, where the linear model can be trained locally with sampled *in situ* or LiDAR data (e.g. GEDI) and then transferred to large scale with TanDEM-X (Schlund et al., 2020). This sampling approach is generally suggested in order to bridge the gap in up-scaling from local to large and even global scale (Réjou-Méchain et al., 2019).

Besides the variation of AGB and its change, other sources of uncertainty are potentially integrated in the field estimations of AGB and its spatial and temporal consistency with the remote sensing data (Réjou-Méchain et al., 2019; Wedeux et al., 2020). The TanDEM-X data was acquired in the same time period of the *in situ* data to maximize temporal consistency. The plots were located in larger areas of homogeneous vegetation, where the forest or plantation structure does not change substantially within the distance of several meters. Consequently, we assume that potential geolocation errors are small. Estimating biomass with labour-intensive plot inventories on the ground is a challenge in itself. The AGB estimates are obtained from allometric equations based on tree height, diameter and wood densities, each one by itself prone to measurement uncertainties depending on the methodology and equipment used and the accuracy in species identification. The AGB uncertainty is in particular not negligible for single trees, but it can be assumed that the errors average out and thus decrease substantially at the plot level where a large number of trees are surveyed (Chave et al., 2014). In addition, the uncertainty and error are at least comparable among studies from similar ecosystems using unified fieldwork protocols and similar calculation approaches such as given in the biomass package (Réjou-Méchain et al., 2017). Even though all observed models were significant and resulted in high accuracies, the number of sample plots was relatively low and the significance and reliability could be further improved by using a larger number of samples in future studies.

4.2. Aboveground biomass change in relation to fires and initial canopy height

Land use and land cover change are not the only causes of biomass loss in tropical regions. Natural and human-caused fires are becoming another key element increasingly shaping vegetation, also in the wet tropics (Cochrane, 2003). Fire is one of the main factors affecting carbon dioxide emissions as well as forest biomass and dynamics in the Amazon basin and other tropical landscapes (van der Werf et al., 2009; Sato et al., 2016; Numata et al., 2017), but few studies are available from South-East Asia. Impacts of fire associated with tree mortality were detected using LiDAR data up to ten years after the fire event, indicating that fire disturbance can cause persistent AGB loss (Sato et al., 2016). Our results confirmed the role of nearby fires for AGB loss, particularly along the borders of old-growth forest and in smallholder plantation landscapes (Langner et al., 2007). This is in line with an increased probability of deforestation closer to fires in the preceding year based on spatially explicit modelling (Armenteras et al., 2017). Therefore, the negative impact of fire occurrence will not yet be outbalanced by potential recovery. This results in the fact that the observed patterns did not change when considering different time intervals of fire occurrence in the ca. 6 year monitoring period (October 30, 2012 to February 25, 2019).

Predominantly during the drier season or after droughts, fires are either naturally ignited or purposefully lit to remove vegetation cover and to make space for new plantations. Dry spells due to extreme El Niño-Southern Oscillations (ENSO) events like the one of 2015–2016 are projected to occur more frequently (Cai et al., 2015; Meijide et al., 2018). Note that about 66% of the observed fires occured in this period. The increase in number and decrease in size of forest fragments may even exacerbate the impacts of drought and consequently fires in the area, as forest remnants are drier and more fire-prone due to higher edge-interior ratios (Cochrane and Laurance, 2002; Laurance, 2004; Numata et al., 2017). Also, compared to primary rainforest, plantations and secondary forests have higher temperatures and vapour pressure deficits and overall lower buffer capacities resulting in higher fire risk (Meijide et al., 2018). In the long term, changing regimes of fire occurrence are expected to alter species composition, favouring herbaceous species and grasses over trees and thus creating fire-mediated positive feedbacks as documented in the Guineo-Congolian rainforest (Cardoso et al., 2018).

Our study confirmed the effects of fires on AGB dynamics in a human-modified tropical landscape known from previous research (Ferraz et al., 2018; Wedeux et al., 2020), demonstrating the potential to quantify their impact on AGB change in different land use systems. Simple models, like the ones used in this study, could be enhanced in the future to model and predict the impact of fires on AGB change and carbon emissions. Interestingly, proximity of fires was associated with AGB loss near the edges of the protected area but not in oil palm concessions where hardly any fires were detected in the time-frame of this study. Oil palm plantations are typically largely devoid of deadwood that could serve as fuel load; only the cropped and stacked palm fronds could be suitable for burning. Furthermore, we consider it likely that these plantations are actively protected from fire ignition and spreading of fire by preventative measures as fires may cause high economic losses.

The initial canopy height in 2012 had an even stronger impact on AGB changes than fires. In general, we found that AGB increases are strongest where initial canopy height is low, whereas areas with tall canopies have mostly lost biomass. Younger trees and pioneer species such as those occurring more frequently in over-logged or secondary forests are known to initially gain biomass quickly before reaching a saturation point at maturity after 80 or even up to 200 years (Wang et al., 2017; Feldpausch et al., 2007). Similar trends can be observed for tree plantations such as rubber, *Acacia* spp. or *Eucalyptus* spp. (Zhang et al., 2012).

The ecosystem restoration concession Hutan Harapan, for which our analyses suggests significant AGB changes, was a timber concession managed by the company PT Asialog until the early 2000s. The company mainly practiced selective logging, and in some areas clear-cutting. Other areas were also reforested by the company using non-native acacia trees. Before the concession was transferred to the conservation company PT REKI in 2010, an establishment of settlements and smallholder plantations started in the north and west of the Hutan Harapan area (Hein, 2018). The expansion of these settlements and associated smallholder farms can explain, to some degree, the negative and positive AGB changes in the Harapan Rainforest area. Smallholder farmers mainly use fire (as they lack financial resources to invest in heavy machinery) to clear forests and shrubs for the establishment of plantations or staple crop cultivation. Positive AGB changes in the Hutan Harapan can be mainly attributed to growing of smallholder oil palm and rubber plantations, recently established agroforestry systems, replanting by PT REKI and natural regrowth of forests in parts of the concession.

The substantial negative AGB changes in oil palm concession areas are mainly caused by the need to replace oil palms approximately 25 years after planting (Luskin and Potts, 2011; Guillaume et al., 2018). This indicates that carbon sequestration effects of oil palm plantations were largely lost in the course of replanting. As our study only extends over the period from 2012 to 2019, we were not able to cover the vast AGB losses that occurred as a result of of logging and the development of large-scale oil palm estates since the 1970s (Laumonier et al., 2010).

5. Conclusions

Our study indicated that AGB changes in a human-modified tropical

landscape can be estimated accurately in terms of RMSE of 2.38 Mg $ha^{-1}year^{-1}$ with TanDEM-X InSAR height changes. This was 13.32% compared to the actual AGB difference range. The compensation of the penetration of the SAR signal into the forest volume improved the relationship in terms of R^2 from 0.53 to 0.65 compared to not-compensated InSAR heights. This suggests that penetration depth and its differences should not be neglected, especially for detecting growth and degradation resulting in small AGB changes. The multiple global coverage of TanDEM-X indicates that this data source has a large potential to estimate AGB changes on large to even global scale. The AGB change estimation could be potentially further improved in the future by using additional information from the TanDEM-X data such as the interferometric coherence and texture information (Schlund et al., 2015; Knapp et al., 2018). The results are also of relevance for future missions like the High Resolution Wide Swath (HRWS) mission with potentially new bistatic InSAR acquisitions (Janoth et al., 2019).

The spatially consistent AGB change information was further used to assess these changes in relation to their initial canopy height and proximity to fires. Our results show that low initial canopy heights tend to be associated with AGB gains while tall initial canopies and proximity to fires tend to be associated with biomass losses. This highlights the importance of spatio-temporal context for AGB dynamics in complex tropical landscapes. Our AGB change estimation technique could be expanded to include other ecosystem processes and thus improve the understanding of drivers of AGB changes. Moreover, the AGB change estimations can be combined in the future with qualitative research to explain the root causes of landscape transformations. Predictive models of fire impacts and carbon emissions based on the AGB change information provided by InSAR height models can be considered high potential data sources in order to support sustainable forest management systems.

CRediT authorship contribution statement

Michael Schlund: Conceptualization, Methodology, Software, Formal analysis, Investigation, Data curation, Writing - original draft, Project administration, Funding acquisition. **Martyna M. Kotowska:** Conceptualization, Methodology, Formal analysis, Investigation, Resources, Data curation, Writing - original draft, Funding acquisition, Project administration. **Fabian Brambach:** Methodology, Formal analysis, Investigation, Resources, Data curation, Writing - original draft. **Jonas Hein:** Resources, Writing - original draft. **Birgit Wessel:** Methodology, Software, Data curation, Writing - Review & Editing. **Nicolò Camarretta:** Resources, Data curation, Writing - Review & Editing. **Mangarah Silalahi:** Data curation, Writing - Review & Editing. **I Nengah Surati Jaya:** Data curation, Writing - Review & Editing. **Stefan Erasmi:** Funding acquisition, Project administration, Writing - Review & Editing. **Christoph Leuschner:** Funding acquisition, Project administration, Writing - Review & Editing. **Holger Kreft:** Funding acquisition, Project administration, Writing - Review & Editing.

Declaration of Competing Interest

The authors declare that they have no known competing financial interests or personal relationships that could have appeared to influence the work reported in this paper.

Acknowledgments

This work was supported in part by the German Federal Ministry for Economic Affairs and Energy (BMWi) through the project IKEBANA with the consortium of University of Göttingen, German Remote Sensing Data Center and Airbus Defence & Space GmbH under Grant 50EE1808 and by the German Research Foundation (DFG) in the framework of the research project EFForTS (CRC990). We thank local assistants for support with fieldwork, as well as village leaders, local plot owners, PT REKI, and the Indonesian Research Foundation (LIPI) for research permissions. This study was conducted using samples collected with the Collection Permits No. 2704/IPH.1/KS.02/X1/2012 and issued by the FRP-Kemenristek. Field work in Jambi province was carried out under research permit numbers 207/SIP/FRP/SM/VI/2012 and 46/E5/E5.4lS—P.EXT/2019. TanDEM-X data used within this work were provided by DLR under proposal XTI_VEGE7394. We acknowledge the use of concession data from the Ministry of Environment and Forestry, Directorate General of Forestry Planning and Environmental Management and the Ministry of Agriculture, Directorate General of Estate Crop, Jakarta, Indonesia. We acknowledge the use of data and/or imagery from NASA's Fire Information for Resource Management System (FIRMS) (https://earthdata.nasa.gov/firms), part of the NASA Earth Observing System Data and Information System (EOSDIS).

References

Armenteras, D., Gibbes, C., Anaya, J.A., Dávalos, L.M., 2017. Integrating remotely sensed fires for predicting deforestation for REDD+. Ecol. Appl. 27 (4), 1294–1304.

Asner, G.P., Mascaro, J., 2014. Mapping tropical forest carbon: Calibrating plot estimates to a simple LiDAR metric. Remote Sens. Environ. 140, 614–624. URL: http://www.sciencedirect.com/science/article/pii/S003442571300360X.

Austin, K.G., Schwantes, A., Gu, Y., Kasibhatla, P.S., feb 2019. What causes deforestation in Indonesia? Environ. Res. Lett. 14 (2), 024007. https://doi.org/10.1088/1748-9326/aaf6db.

Beer, C., Reichstein, M., Tomelleri, E., Ciais, P., Jung, M., Carvalhais, N., Rödenbeck, C., Arain, M.A., Baldocchi, D., Bonan, G.B., 2010. Terrestrial gross carbon dioxide uptake: global distribution and covariation with climate. Science 329 (5993), 834–838.

Brun, C., Cook, A.R., Lee, J.S.H., Wich, S.A., Koh, L.P., Carrasco, L.R., 2015. Analysis of deforestation and protected area effectiveness in Indonesia: A comparison of Bayesian spatial models. Global Environ. Change 31, 285–295.

Cai, W., Santoso, A., Wang, G., Yeh, S.-W., An, S.-I., Cobb, K.M., Collins, M., Guilyardi, E., Jin, F.-F., Kug, J.-S., Lengaigne, M., McPhaden, M.J., Takahashi, K., Timmermann, A., Vecchi, G., Watanabe, M., Wu, L., 2015. ENSO and greenhouse warming. Nature Climate Change 5 (9), 849–859 number: 9 Publisher: Nature Publishing Group. URL: https://www.nature.com/articles/nclimate2743.

Cao, L., Coops, N.C., Innes, J.L., Sheppard, S.R., Fu, L., Ruan, H., She, G., 2016. Estimation of forest biomass dynamics in subtropical forests using multi-temporal airborne LiDAR data. Remote Sens. Environ. 178, 158–171. URL: http://www.sciencedirect.com/science/article/pii/S0034425716301067.

Cardoso, A.W., Oliveras, I., Abernethy, K.A., Jeffery, K.J., Lehmann, D., Edzang Ndong, J., McGregor, I., Belcher, C.M., Bond, W.J., Malhi, Y.S., 2018. Grass species flammability, not biomass, drives changes in fire behavior at tropical forest-savanna transitions. Front. Forests Global Change 1, 6.

Chave, J., Coomes, D., Jansen, S., Lewis, S.L., Swenson, N.G., Zanne, A.E., 2009. Towards a worldwide wood economics spectrum. Ecol. Lett. 12 (4), 351–366.

Chave, J., Réjou-Méchain, M., Búrquez, A., Chidumayo, E., Colgan, M.S., Delitti, W.B.C., Duque, A., Eid, T., Fearnside, P.M., Goodman, R.C., 2014. Improved allometric models to estimate the aboveground biomass of tropical trees. Glob. Change Biol. 20 (10), 3177–3190.

Chen, Q., Vaglio Laurin, G., Valentini, R., 2015. Uncertainty of remotely sensed aboveground biomass over an African tropical forest: Propagating errors from trees to plots to pixels. Remote Sens. Environ. 160, 134–143. URL: https://www.sciencedirect.com/science/article/pii/S0034425715000188.

Chhatre, A., Agrawal, A., 2009. Trade-offs and synergies between carbon storage and livelihood benefits from forest commons. Proc. Nat. Acad. Sci. 106 (42), 17667–17670. URL: https://www.pnas.org/content/106/42/17667.

Clough, Y., Krishna, V.V., Corre, M.D., Darras, K., Denmead, L.H., Meijide, A., Moser, S., Musshoff, O., Steinebach, S., Veldkamp, E., Allen, K., Barnes, A.D., Breidenbach, N., Brose, U., Buchori, D., Daniel, R., Finkeldey, R., Harahap, I., Hertel, D., Holtkamp, A. M., Hörandl, E., Irawan, B., Jaya, I.N.S., Jochum, M., Klarner, B., Knohl, A., Kotowska, M.M., Krashevska, V., Kreft, H., Kurniawan, S., Leuschner, C., Maraun, M., Melati, D.N., Opfermann, N., Pérez-Cruzado, C., Prabowo, W.E., Rembold, K., Rizali, A., Rubiana, R., Schneider, D., Tjitrosoedirdjo, S.S., Tjoa, A., Tscharntke, T., Scheu, S., 2016. Land-use choices follow profitability at the expense of ecological functions in Indonesian smallholder landscapes. Nat. Commun. 7 (13137), 1–12.

Cochrane, M.A., 2003. Fire science for rainforests. Nature 421 (6926), 913–919.

Cochrane, M.A., Laurance, W.F., 2002. Fire as a large-scale edge effect in Amazonian forests. J. Trop. Ecol. 311–325.

Curtis, P.G., Slay, C.M., Harris, N.L., Tyukavina, A., Hansen, M.C., 2018. Classifying drivers of global forest loss. Science 361 (6407), 1108–1111.

Dall, J., 2007. InSAR elevation bias caused by penetration into uniform volumes. IEEE Trans. Geosci. Remote Sens. 45 (7), 2319–2324.

Daskalova, G.N., Myers-Smith, I.H., Bjorkman, A.D., Blowes, S.A., Supp, S.R., Magurran, A.E., Dornelas, M., 2020. Landscape-scale forest loss as a catalyst of population and biodiversity change. Science 368 (6497), 1341–1347. URL: https://science.sciencemag.org/content/368/6497/1341.

Drescher, J., Rembold, K., Allen, K., Beckschäfer, P., Buchori, D., Clough, Y., Faust, H., Fauzi, A.M., Gunawan, D., Hertel, D., Irawan, B., Jaya, I.N.S., Klarner, B., Kleinn, C., Knohl, A., Kotowska, M.M., Krashevska, V., Krishna, V., Leuschner, C., Lorenz, W., Meijide, A., Melati, D., Nomura, M., Pérez-Cruzado, C., Qaim, M., Siregar, I.Z., Steinebach, S., Tjoa, A., Tscharntke, T., Wick, B., Wiegand, K., Kreft, H., Scheu, S., 2016. Ecological and socio-economic functions across tropical land use systems after rainforest conversion. Philosoph. Trans. Roy. Soc. B: Biol. Sci. 371 (1694), 20150275. URL: https://royalsocietypublishing.org/doi/abs/10.1098/rstb.2015.0275.

Dubayah, R.O., Sheldon, S.L., Clark, D.B., Hofton, M.A., Blair, J.B., Hurtt, G.C., Chazdon, R.L., 2010. Estimation of tropical forest height and biomass dynamics using lidar remote sensing at La Selva, Costa Rica. J. Geophys. Res.: Biogeosci. 115 (G2). URL: https://agupubs.onlinelibrary.wiley.com/doi/abs/10.1029/2009JG000933.

Feintrenie, L., Levang, P., 2009. Sumatra's Rubber Agroforests: Advent, Rise and Fall of a Sustainable Cropping System. Small-scale Forestry 8 (3), 323–335. https://doi.org/10.1007/s11842-009-9086-2.

Feldpausch, T.R., Prates-Clark, C. d.C., Fernandes, E.C., Riha, S.J., 2007. Secondary forest growth deviation from chronosequence predictions in central Amazonia. Global Change Biol. 13 (5), 967–979.

Ferraz, A., Saatchi, S., Xu, L., Hagen, S., Chave, J., Yu, Y., Meyer, V., Garcia, M., Silva, C., Roswintiart, O., Samboko, A., Sist, P., Walker, S., Pearson, T.R.H., Wijaya, A., Sullivan, F.B., Rutishauser, E., Hoekman, D., Ganguly, S., aug 2018. Carbon storage potential in degraded forests of Kalimantan, Indonesia. Environ. Res. Lett. 13 (9), 095001. https://doi.org/10.1088/1748-9326/aad782.

Fritz, T., 2012. TanDEM-X. Ground Segment. TanDEM-X Experimental Product Description. Issue: 1.2. Deutsches Zentrum fuer Luft- und Raumfahrt (DLR), Oberpfaffenhofen.

Fritz, T., Rossi, C., Yague-Martinez, N., Rodriguez-Gonzalez, F., Lachaise, M., Breit, H., 2011. Interferometric processing of TanDEM-X data. In: 2011 IEEE International Geoscience and Remote Sensing Symposium, pp. 2428–2431.

Giglio, L., Descloitres, J., Justice, C.O., Kaufman, Y.J., 2003. An Enhanced Contextual Fire Detection Algorithm for MODIS. Remote Sens. Environ. 87 (2), 273–282. URL: http://www.sciencedirect.com/science/article/pii/S0034425703001846.

Gruber, A., Wessel, B., Huber, M., Roth, A., 2012. Operational TanDEM-X DEM calibration and first validation results. ISPRS J. Photogramm. Remote Sensing 73, 39–49, innovative Applications of SAR Interferometry from modern Satellite Sensors. URL: http://www.sciencedirect.com/science/article/pii/S0924271612001037.

Guillaume, T., Kotowska, M.M., Hertel, D., Knohl, A., Krashevska, V., Murtilaksono, K., Scheu, S., Kuzyakov, Y., 2018. Carbon costs and benefits of Indonesian rainforest conversion to plantations. Nautre Commun. 9 (2388), 1–11.

Hein, J., 2018. Political Ecology of REDD+ in Indonesia: Agrarian Conflicts and Forest Carbon, 1st ed. Routledge, London.

Hein, J., Adiwibowo, S., Dittrich, C., Rosyani, Soetarto, E., Faust, H., 2016. Rescaling of Access and Property Relations in a Frontier Landscape: Insights from Jambi, Indonesia. Professional Geographer 68 (3), 380–389. https://doi.org/10.1080/00330124.2015.1089105.

Hudak, A.T., Strand, E.K., Vierling, L.A., Byrne, J.C., Eitel, J.U., Martinuzzi, S., Falkowski, M.J., 2012. Quantifying aboveground forest carbon pools and fluxes from repeat LiDAR surveys. Remote Sens. Environ. 123, 25–40. URL: http://www.sciencedirect.com/science/article/pii/S0034425712001162.

Janoth, J., Jochum, M., Petrat, L., Knigge, T., 2019. High Resolution wide Swath - the Next Generation X-Band Mission. In: IEEE International Geoscience and Remote Sensing Symposium (IGARSS), pp. 3535–3537.

Karila, K., Yu, X., Vastaranta, M., Karjalainen, M., Puttonen, E., Hyyppä, J., 2019. TanDEM-X digital surface models in boreal forest above-ground biomass change detection. ISPRS J. Photogramm. Remote Sensing 148, 174–183. URL: http://www.sciencedirect.com/science/article/pii/S0924271619300024.

Khasanah, N., van Noordwijk, M., Ningsih, H., 2015. Aboveground carbon stocks in oil palm plantations and the threshold for carbon-neutral vegetation conversion on mineral soils. Cogent Environmental. Science 1 (1). https://doi.org/10.1080/23311843.2015.1119964.

Knapp, N., Huth, A., Kugler, F., Papathanassiou, K., Condit, R., Hubbell, S.P., Fischer, R., 2018. Model-Assisted Estimation of Tropical Forest Biomass Change: A Comparison of Approaches. Remote Sensing 10 (5), 1–23.

Kotowska, M.M., Leuschner, C., Triadiati, T., Meriem, S., Hertel, D., 2015. Quantifying above- and belowground biomass carbon loss with forest conversion in tropical lowlands of Sumatra (Indonesia). Glob. Change Biol. 21 (10), 3620–3634. URL: https://onlinelibrary.wiley.com/doi/abs/10.1111/gcb.12979.

Krieger, G., Moreira, A., Fiedler, H., Hajnsek, I., Werner, M., Younis, M., Zink, M., nov. 2007. TanDEM-X: A Satellite Formation for High-Resolution SAR Interferometry. IEEE Trans. Geosci. Remote Sens. 45 (11), 3317–3341.

Kugler, F., Schulze, D., Hajnsek, I., Pretzsch, H., Papathanassiou, K., 10 2014. TanDEM-X Pol-InSAR Performance for Forest Height Estimation. IEEE Trans. Geosci. Remote Sens. 52 (10), 6404–6422.

Kvalseth, T.O., 1985. Cautionary Note about R2. Am. Statist. 39 (4), 279–285.

Lachaise, M., Bachmann, M., Fritz, T., Huber, M., Schweißhelm, B., Wessel, B., 2019. Generation Of the Tandem-X Change Dem From the New Global Acquisitions (2017–2019). In: IGARSS 2019–2019 IEEE International Geoscience and Remote Sensing Symposium, pp. 4480–4483.

Langner, A., Miettinen, J., Siegert, F., 2007. Land cover change 2002–2005 in Borneo and the role of fire derived from MODIS imagery. Glob. Change Biol. 13 (11), 2329–2340. https://doi.org/10.1111/j.1365-2486.2007.01442.x.

Laumonier, Y., Uryu, Y., Stüwe, M., Budiman, A., Setiabudi, B., Hadian, O., Apr. 2010. Eco-floristic sectors and deforestation threats in Sumatra: identifying new conservation area network priorities for ecosystem-based land use planning. Biodivers. Conserv. 19 (4), 1153–1174. URL: http://link.springer.com/10.1007/s10531-010-9784-2.

Laurance, W.F., 2004. Forest-climate interactions in fragmented tropical landscapes. Philosoph. Trans. Roy. Soc. London. Series B: Biol. Sci. 359 (1443), 345–352.

Lawrence, D., Vandecar, K., 2015. Effects of tropical deforestation on climate and agriculture. Nature Climate Change 5 (1), 27–36.

Lüdecke, D., Ben-Shachar, M.S., Patil, I., Waggoner, P., Makowski, D., 2021. performance: An R Package for Assessment, Comparison and Testing of Statistical Models. J. Open Source Softw. 6 (60), 3139.

Lei, Y., Treuhaft, R., Keller, M., dos Santos, M., Gonçalves, F., Neumann, M., 2018. Quantification of selective logging in tropical forest with spaceborne SAR interferometry. Remote Sens. Environ. 211, 167–183. URL: http://www.sciencedirect.com/science/article/pii/S0034425718301548.

Lewis, S.L., Edwards, D.P., Galbraith, D., 2015. Increasing human dominance of tropical forests. Science 349 (6250), 827–832.

Luskin, M.S., Potts, M.D., 2011. Microclimate and habitat heterogeneity through the oil palm lifecycle. Basic Appl. Ecol. 12 (6), 540–551. URL: https://www.sciencedirect.com/science/article/pii/S1439179111000764.

Malhi, Y., Grace, J., 2000. Tropical forests and atmospheric carbon dioxide. Trends Ecol. Evol. 15 (8), 332–337.

McRoberts, R.E., Næsset, E., Gobakken, T., Bollandsås, O.M., 2015. Indirect and direct estimation of forest biomass change using forest inventory and airborne laser scanning data. Remote Sens. Environ. 164, 36–42. URL: https://www.sciencedirect.com/science/article/pii/S0034425715000772.

Meijide, A., Badu, C.S., Moyano, F., Tiralla, N., Gunawan, D., Knohl, A., 2018. Impact of forest conversion to oil palm and rubber plantations on microclimate and the role of the 2015 ENSO event. Agric. Forest Meteorol. 252, 208–219.

Mets, K.D., Armenteras, D., Dávalos, L.M., 2017. Spatial autocorrelation reduces model precision and predictive power in deforestation analyses. Ecosphere 8 (5), e01824. URL: https://esajournals.onlinelibrary.wiley.com/doi/abs/10.1002/ecs2.1824.

Meyer, V., Saatchi, S.S., Chave, J., Dalling, J.W., Bohlman, S., Fricker, G.A., Robinson, C., Neumann, M., Hubbell, S., 2013. Detecting tropical forest biomass dynamics from repeated airborne lidar measurements. Biogeosciences 10 (8), 5421–5438. URL: https://bg.copernicus.org/articles/10/5421/2013/.

Nakagawa, S., Johnson, P.C.D., Schielzeth, H., 2017. The coefficient of determination r^2 and intra-class correlation coefficient from generalized linear mixed-effects models revisited and expanded. J. Roy. Soc. Interface 14 (134), 20170213. URL: https://royalsocietypublishing.org/doi/abs/10.1098/rsif.2017.0213.

Numata, I., Silva, S.S., Cochrane, M.A., D'Oliveira, M.V.N., 2017. Fire and edge effects in a fragmented tropical forest landscape in the southwestern Amazon. For. Ecol. Manage. 401, 135–146.

Pan, Y., Birdsey, R.A., Fang, J., Houghton, R., Kauppi, P.E., Kurz, W.A., Phillips, O.L., Shvidenko, A., Lewis, S.L., Canadell, J.G., Ciais, P., Jackson, R.B., Pacala, S.W., McGuire, A.D., Piao, S., Rautiainen, A., Sitch, S., Hayes, D., 2011. A Large and Persistent Carbon Sink in the World's Forests. Science 333 (6045), 988–993.

Pinheiro, J., Bates, D., DebRoy, S., Sarkar, D., R Core Team, 2021. nlme: Linear and Nonlinear Mixed Effects Models. R package version 3.1-152. URL: https://CRAN.R-project.org/package=nlme.

R Core Team, 2021. R: A Language and Environment for Statistical Computing. R Foundation for Statistical Computing, Vienna. URL: http://www.R-project.org/.

Réjou-Méchain, M., Barbier, N., Couteron, P., Ploton, P., Vincent, G., Herold, M., Mermoz, S., Saatchi, S., Chave, J., de Boissieu, F., Féret, J.-B., Takoudjou, S.M., Pélissier, R., 2019. Upscaling Forest Biomass from Field to Satellite Measurements: Sources of Errors and Ways to Reduce Them. Surv. Geophys. 40, 881–911.

Réjou-Méchain, M., Tanguy, A., Piponiot, C., Chave, J., Hérault, B., 2017. biomass: an r package for estimating above-ground biomass and its uncertainty in tropical forests. Methods Ecol. Evol. 8 (9), 1163–1167. URL: https://besjournals.onlinelibrary.wiley.com/doi/abs/10.1111/2041-210X.12753.

Réjou-Méchain, M., Tymen, B., Blanc, L., Fauset, S., Feldpausch, T.R., Monteagudo, A., Phillips, O.L., Richard, H., Chave, J., 2015. Using repeated small-footprint LiDAR acquisitions to infer spatial and temporal variations of a high-biomass Neotropical forest. Remote Sens. Environ. 169, 93–101. URL: http://www.sciencedirect.com/science/article/pii/S0034425715300894.

Rizzoli, P., Martone, M., Gonzalez, C., Wecklich, C., Tridon, D.B., Bräutigam, B., Bachmann, M., Schulze, D., Fritz, T., Huber, M., Wessel, B., Krieger, G., Zink, M., Moreira, A., 2017. Generation and performance assessment of the global TanDEM-X digital elevation model. ISPRS J. Photogramm. Remote Sensing 132, 119–139. URL: http://www.sciencedirect.com/science/article/pii/S092427161730093X.

Rossi, C., Rodriguez Gonzalez, F., Fritz, T., Yague-Martinez, N., Eineder, M., 2012. TanDEM-X calibrated Raw DEM generation. ISPRS Journal of Photogrammetry and Remote Sensing 73, 12–20, innovative Applications of SAR Interferometry from modern Satellite Sensors. URL: http://www.sciencedirect.com/science/article/pii/S0924271612001062.

Sato, L.Y., Gomes, V.C.F., Shimabukuro, Y.E., Keller, M., Arai, E., Dos-Santos, M.N., Brown, I.F., 2016. Post-fire changes in forest biomass retrieved by airborne LiDAR in Amazonia. Remote Sensing 8 (10), 839.

Schlund, M., Baron, D., Magdon, P., Erasmi, S., 2019. Canopy penetration depth estimation with TanDEM-X and its compensation in temperate forests. ISPRS J. Photogramm. Remote Sensing 147, 232–241. URL: http://www.sciencedirect.com/science/article/pii/S0924271618303228.

Schlund, M., Erasmi, S., Scipal, K., March 2020. Comparison of Aboveground Biomass Estimation From InSAR and LiDAR Canopy Height Models in Tropical Forests. IEEE Geosci. Remote Sens. Lett. 17 (3), 367–371.

Schlund, M., von Poncet, F., Kuntz, S., Schmullius, C., Hoekman, D.H., 2015. TanDEM-X data for aboveground biomass retrieval in a tropical peat swamp forest. Remote

Sens. Environ. 158, 255–266. URL: http://www.sciencedirect.com/science/article/pii/S0034425714004581.
Schroeder, W., Oliva, P., Giglio, L., Csiszar, I.A., 2014. The New VIIRS 375m active fire detection data product: Algorithm description and initial assessment. Remote Sens. Environ. 143, 85–96. URL: http://www.sciencedirect.com/science/article/pii/S0034425713004483.
Solberg, S., Astrup, R., Breidenbach, J., Nilsen, B., Weydahl, D., 2013. Monitoring spruce volume and biomass with InSAR data from TanDEM-X. Remote Sens. Environ. 139, 60–67.
Solberg, S., Gizachew, B., Naesset, E., Gobakken, T., Bollandsas, O.M., Mauya, E.W., Olsson, H., Malimbwi, R., Zahabu, E., Jun 2015. Monitoring forest carbon in a Tanzanian woodland using interferometric SAR: a novel methodology for REDD+. Carbon Balance Manage. 10 (1), 14. https://doi.org/10.1186/s13021-015-0023-8.
Solberg, S., May, J., Bogren, W., Breidenbach, J., Torp, T., Gizachew, B., 2018. Interferometric SAR DEMs for Forest Change in Uganda 2000–2012. Remote Sensing 10 (2), 1–17.
Solberg, S., Naesset, E., Gobakken, T., Bollandsas, O.-M., 2014. Forest biomass change estimated from height change in interferometric SAR height models. Carbon Balance Manage. 9 (1), 5. https://doi.org/10.1186/s13021-014-0005-2.
Tompalski, P., Coops, N.C., White, J.C., Goodbody, T.R., Hennigar, C.R., Wulder, M.A., Socha, J., Woods, M.E., 2021. Estimating Changes in Forest Attributes and Enhancing Growth Projections: a Review of Existing Approaches and Future Directions Using Airborne 3D Point Cloud Data. Current Forestry Reports.
Treuhaft, R.N., Siqueira, P.R., 2004. The calculated performance of forest structure and biomass estimates from interferometric radar. Waves Random Media 14 (2), 345–358.
van der Werf, G.R., Morton, D.C., DeFries, R.S., Olivier, J.G.J., Kasibhatla, P.S., Jackson, R.B., Collatz, G.J., Randerson, J.T., 2009. CO2 emissions from forest loss. Nat. Geosci. 2, 737–738.
Venter, O., Sanderson, E.W., Magrach, A., Allan, J.R., Beher, J., Jones, K.R., Possingham, H.P., Laurance, W.F., Wood, P., Fekete, B.M., 2016. Sixteen years of change in the global terrestrial human footprint and implications for biodiversity conservation. Nature Commun. 7 (1), 1–11.
Wang, F., Ding, Y., Sayer, E.J., Li, Q., Zou, B., Mo, Q., Li, Y., Lu, X., Tang, J., Zhu, W., Li, Z., 2017. Tropical forest restoration: Fast resilience of plant biomass contrasts with slow recovery of stable soil C stocks. Funct. Ecol. 31 (12), 2344–2355. URL: https://besjournals.onlinelibrary.wiley.com/doi/abs/10.1111/1365-2435.12925.
Watson, J.E.M., Evans, T., Venter, O., Williams, B., Tulloch, A., Stewart, C., Thompson, I., Ray, J.C., Murray, K., Salazar, A., 2018. The exceptional value of intact forest ecosystems. Nature Ecol. Evol. 2 (4), 599–610.
Wedeux, B., Dalponte, M., Schlund, M., Hagen, S., Cochrane, M., Graham, L., Usup, A., Thomas, A., Coomes, D., 2020. Dynamics of a human-modified tropical peat swamp forest revealed by repeat lidar surveys. Glob. Change Biol. 26 (7), 3947–3964. URL: https://onlinelibrary.wiley.com/doi/abs/10.1111/gcb.15108.
Wessel, B., Huber, M., Wohlfart, C., Marschalk, U., Kosmann, D., Roth, A., 2018. Accuracy assessment of the global TanDEM-X Digital Elevation Model with GPS data. ISPRS J. Photogramm. Remote Sens. 139, 171–182. URL: http://www.sciencedirect.com/science/article/pii/S0924271618300522.
Zanne, A.E., Lopez-Gonzalez, G., Coomes, D.A., Ilic, J., Jansen, S., Lewis, S.L., Miller, R. B., Swenson, N.G., Wiemann, M.C., Chave, J., 2009. Data from: Towards a worldwide wood economics spectrum. Dryad, Dataset.
Zhang, H., Guan, D., Song, M., 2012. Biomass and carbon storage of Eucalyptus and Acacia plantations in the Pearl River Delta, South China. For. Ecol. Manage. 277, 90–97. URL: https://www.sciencedirect.com/science/article/pii/S0378112712002241.